Available online at www.sciencedirect.com
ScienceDirect
Trans. Nonferrous Met. Soc. China 33(2023) 824−838
Transactions of Nonferrous Metals Society of China
www.tnmsc.cn

Experimental investigation and thermodynamic modeling of Cu–Nb–Si system

Jia-qiang ZHOU[1,2], Biao HU[1,3], Ben-fu LI[1,3], Yong DU[2], Jiong WANG[2]

1. School of Materials Science and Engineering, Anhui University of Science and Technology, Huainan 232001, China;
2. State Key Laboratory of Powder Metallurgy, Central South University, Changsha 410083, China;
3. Anhui International Joint Research Center for Nano Carbon-based Materials and Environmental Health, Huainan 232001, China

Received 14 October 2021; accepted 2 January 2022

Abstract: The phase equilibria of the Cu–Nb–Si system were investigated via a combination of key equilibrated alloys, thermodynamic modeling and first-principles calculations. Sixteen ternary alloys were prepared to determine the isothermal sections at 600 and 700 °C, by means of X-ray diffraction (XRD) and scanning electron microscopy with energy dispersive X-ray spectroscopy (SEM−EDS). The three- and two-phase regions were determined. The existence of ternary compound τ_1 ($Cu_4Nb_5Si_4$) was confirmed. The solubilities of Cu in the $NbSi_2$ and Nb_5Si_3 phases were measured. Based on the experimental equilibria data from the literature and the present work, a thermodynamic description of the Cu–Nb–Si system was carried out by using the calculation of phase diagrams (CALPHAD) method supported by first-principles calculations. The substitutional model and sublattice model were employed to describe the solution phases and intermediate phases, respectively. A set of self-consistent thermodynamic parameters of the Cu–Nb–Si system were conclusively obtained. Most of the reliable experimental data were reproduced by the present thermodynamic modeling.

Key words: Cu–Nb–Si system; thermodynamic modeling; first-principles calculations; CALPHAD approach

1 Introduction

Cu-based alloys exhibit the excellent characteristics such as high electrical conductivity, superior thermal conductivity, and good mechanical properties [1−4], which are widely used in electricity, microelectronics, aerospace, ocean transport and other fields. The high electrical conductivity and high thermal conductivity are the most important characteristics of copper. However, pure Cu with low mechanical properties cannot service in a high-temperature environment for a long time, which can be enhanced by adding alloying elements, such as Nb and Si [5]. Nb can also improve the thermal stability of the Cu-based alloy [6,7]. Nb_5Si_3_L and $NbSi_2$ are two promising candidate materials for the next generation of high-temperature parts such as the hot sections of aircraft and spacecraft engines, due to their high melting points, low densities and exceptional mechanical performance at the temperatures above 1200 °C [8−10]. The development of the new copper alloy requires information about the phase equilibria and thermodynamic properties of the Cu-based ternary systems.

Corresponding author: Biao HU, Tel/Fax: +86-554-6601194, E-mail: hubiao05047071@163.com;
Jiong WANG, Tel/Fax: +86-731-88877300, E-mail: wangjionga@csu.edu.cn
DOI: 10.1016/S1003-6326(23)66149-7

The accurate thermodynamic descriptions of the Cu-based ternary systems were considerable efforts of our group to establish a thermodynamic database for the multicomponent Cu-based alloys [11−16]. However, to the best of our knowledge, there is no thermodynamic modeling of the Cu−Nb−Si ternary system available in the literature. There are no reports on the thermodynamic modeling of the Cu−Nb−Si ternary system, and the experimental phase equilibria data are also scattered. Thus, the objectives of the present work are: (1) to determine the phase equilibria of the Cu−Nb−Si system at 600 and 700 °C by XRD and SEM−EDS, (2) to perform first-principles calculations to obtain the enthalpies of formation at 0 K for the end-members of $NbSi_2$ and Nb_5Si_3_L and the ternary compounds τ_1 and τ_2, and (3) to obtain a set of self-consistent thermodynamic parameters for the Cu−Nb−Si system by the CALPHAD approach [17,18]. In summary, the present studies on the thermodynamic assessment of the Cu−Nb−Si system are extremely useful for providing a set of reliable thermodynamic parameters for thermodynamic extrapolations to related higher order systems. And the copper alloy database established by our group can provide the theoretical basis for material research and process control, especially for the development of new copper alloys.

2 Literature review

Both the experimental data of the Cu−Nb−Si system published in the literature [19−22] are critically evaluated below. To facilitate reading, the symbols used to denote the phases with their crystal structures in the Cu−Nb−Si system are listed in Table 1, and the investigations on phase equilibria and crystal structures used in the optimization are summarized in Table 2.

2.1 Cu−Si system

The Cu−Si phase diagram was very complex with a number of intermediate phases in the Cu-rich part at different temperatures. The Cu−Si system has been thermodynamically described several times [31−34]. All thermodynamic models could reproduce the phase diagram well. New experimental investigations with focus on the Cu-rich part were performed by HALLSTEDT et al [34] and SUFRYD et al [35]. Most recently, thermodynamic evaluation of the system was proposed by HALLSTEDT et al [34] which considered more recent experimental data [35] and their own calorimetric measurements data. However, the thermodynamic parameters proposed by HALLSTEDT et al [34] were incompatible with the ones in our constructed Cu alloys thermodynamic

Table 1 Phase in Cu−Nb−Si system

Phase	Prototype	Pearson symbol	Space group	Phase description	Ref.
(Cu)	Cu	*cF*4	$Fm\bar{3}m$	Solid solution based on fcc Cu	[23]
(Nb)	W	*cI*2	$Im\bar{3}m$	Solid solution based on bcc Nb	[23]
bcc(CuSi)	–	*cI*2	$Im\bar{3}m$	Solid solution based on bcc(CuSi)	[24]
(Si)	C	*cF*8	$Fd\bar{3}m$	Solid solution based on diamond Si	[23]
hcp(CuSi)	Mg	*hP*2	$P6_3/mmc$	Solid solution based on hcp(CuSi)	[24]
Nb_5Si_3_L	Cr_5Si_3	*tI*32	*I*4/*mcm*	Binary compound Nb_5Si_3 at high-temperature	[25]
Nb_5Si_3_H	W_5Si_3	*tI*32	*I*4/*mcm*	Binary compound Nb_5Si_3 at low-temperature	[25]
Nb_3Si	PTi_3	*tP*32	P_4/n	Binary compound Nb_3Si	[26]
$NbSi_2$	$CrSi_2$	*hP*9	$P6_222$	Binary compound $NbSi_2$	[27]
$Cu_{15}Si_4$	$Cu_{15}Si_4$	*cI*76	$I\bar{4}3d$	Binary compound $Cu_{15}Si_4$	[28]
$Cu_{19}Si_6$	–	hR*	$R\bar{3}m$	Binary compound $Cu_{19}Si_6$	[29]
$Cu_{56}Si_{11}$	β-Mn	*cP*20	$P4_132$	Binary compound $Cu_{56}Si_{11}$	[24]
$Cu_{33}Si_7$	–	*tP**	–	Binary compound $Cu_{33}Si_7$	[30]
τ_1	$Nb_5Cu_4Si_4$	*tI*26	*I*4/*m*	Ternary compound $Nb_5Cu_4Si_4$	[19]
τ_2	Nb_4CoSi	*tP*12	*P*4/*mmc*	Ternary compound Nb_4CuSi	[22]

Table 2 Phase diagram and thermodynamic data for Cu–Nb–Si system available in literature

Technique[a]	Type of data	QM[b]	Ref.
XRD	Crystal structure of ternary τ_1 phase	■	[19]
OM, XRD, MD	Isothermal section at 800 °C	□	[20]
	Confirming that τ_1 phase exists	■	[20]
OM, XRD, EMPA	Isothermal section at 800 °C	□	[21]
	Isothermal section at 875 °C	□	[21]
	Presenting liquidus surface	□	[21]
	Reporting that τ_1 does not exist	□	[21]
OM, XRD	Isothermal section at 1500 °C	○	[22]
	Crystal structure of ternary τ_2 phase	■	[22]
	τ_2 formed above 1500 °C	○	[22]

[a] XRD: X-ray diffraction; OM: Optical metallography; MD: microhardness; EMPA: Electron probe micro-analyzer;
[b] QM: Quoted Mode, indicating whether the data are used in the parameter: ■ used; □ not used; ○ not used but estimated to be reliable data for checking the modeling

database. The CALPHAD description for the Cu−Si system from YAN and CHANG [36] provided a good description of the experimental data, and was successfully used to establish the thermodynamic database for Al-based alloys [37]. Thus, the thermodynamic parameters from YAN and CHANG [36] were adopted in the present work. The calculated phase diagram of the Cu−Si system is shown in Fig. 1(a).

2.2 Si−Nb system

The Si−Nb binary system contains four compounds, i.e., $NbSi_2$, Nb_5Si_3_L, Nb_5Si_3_H and Nb_3Si. The Si−Nb binary system has been thermodynamically evaluated [25,26,39−42]. In general, the calculated phase diagrams are very similar, except that a different thermodynamic model was used to describe the range of homogeneity of compounds. Recently, the Si−Nb system was thermodynamically assessed by GENG et al [26] accounting for the homogeneity ranges of compounds, and their calculated results can reproduce experimental information satisfactorily. The assessment performed by GENG et al [26] was directly adopted in the present work, and the calculated Si–Nb phase diagram is shown in Fig. 1(b).

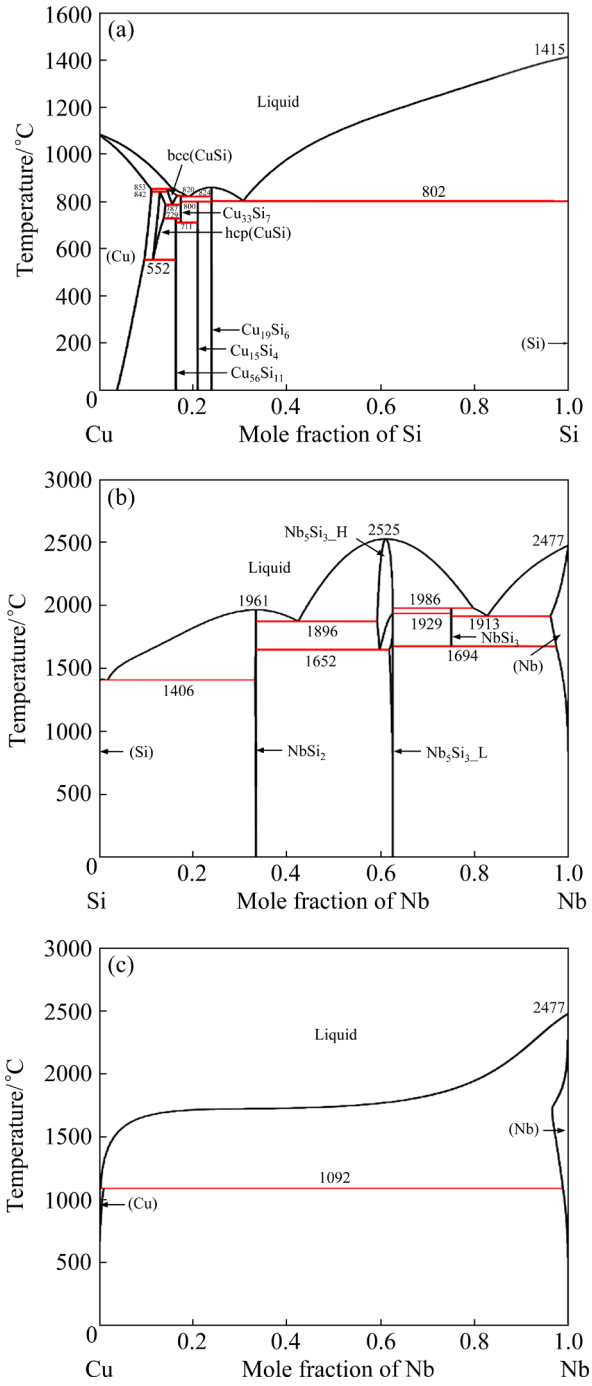

Fig. 1 Calculated Cu−Si (a), Si−Nb (b), and Cu−Nb (c) phase diagrams using thermodynamic parameters from YAN and CHANG [36], GENG et al [26], and HÄMÄLÄINEN et al [38], respectively

2.3 Cu−Nb system

The phase equilibria of the Cu−Nb system was characterized by only one invariant reaction with extremely limited solubility. Some authors [43−46] suggested that the invariant reaction was a monotectic type, whereas other authors [47−50] believed this reaction to be the peritectic type.

Investigators [48−50] claimed that the monotectic invariant reaction observed by the authors [43−46] was due to the effect of impurities. The thermodynamic assessment of the Cu−Nb system was only performed by HÄMÄLÄINEN et al [38]. And the reaction in phase equilibria was calculated to the peritectic type. The thermodynamic parameters obtained by HÄMÄLÄINEN et al [38] were adopted in the present work. Figure 1(c) presents the calculated phase diagram of the Cu−Nb system using the thermodynamic description of HÄMÄLÄINEN et al [38].

2.4 Cu−Nb−Si ternary system

By XRD analysis, GANGLBERGER [19] first detected the new ternary phase τ_1 ($Cu_4Nb_5Si_4$) in the Cu−Nb−Si alloy and determined the crystal structure (space group $I4/m$, lattice parameters a=10.19 Å, and c=3.60 Å). Then, combining XRD, optical metallography (OM) and micro hardness measurements, SAVITSKII et al [20] determined one three-phase region (Cu) + (Nb) + τ_1 in the isothermal section at 800 °C and also determined the crystal structure of the τ_1 ternary compound. However, the stability of the ternary phase τ_1 was discussed controversially in literature [19−21]. By employing OM, XRD and electron probe micro-analyzer (EMPA), ZANKL and MALTER [21] constructed the isothermal sections at 800 and 875 °C. However, the τ_1 phase was not observed. ZANKL and MALTER [21] claimed that the τ_1 phase was a metastable phase and explained the appearance of τ_1 by non- equilibrium crystallization conditions. Subsequently, PAN et al [22] measured the partial phase equilibria at 1500 °C in the Nb-rich region by using OM and XRD. The new ternary phase τ_2 (Nb_4CuSi) was identified with Nb_4CoSi type structure (space group $P4/mmc$, lattice parameters a=3.60 Å, and c=6.21 Å) with a limited homogeneity range of Cu. The solubility of Cu in Nb_5Si_3 was also measured to be 12 at.% in their work. Furthermore, REID et al [51] tentatively calculated the phase equilibria of the Cu−Nb−Si system at 700 °C, but they did not take into account the ternary compounds. According to the evaluation of experimental data of the Cu−Nb−Si system, the experimental results of SAVITSKII et al [20] were inconsistent with the ones from ZANKL and MALTER [21], and the phase equilibria at 800 and 1500 °C measured in the literature [20,22] have not been completely determined. Thus, there are still some issues to be resolved. On the one hand, the existence of ternary phase τ_1 needs to be clarified. On the other hand, the composition ranges of the $Cu_{19}Si_6$, $Cu_{15}Si_4$, $Cu_{56}Si_{11}$, $NbSi_2$, Nb_5Si_3 and τ_1 phases needs to be determined by the key experiments. Then, the thermodynamic assessment of the Cu−Nb−Si system could be performed by taking into consideration of the experimental data available in the literature and present work as well as the enthalpies of formation values from the first-principles calculations.

3 Experimental

The phase equilibria of the Cu−Nb−Si systems at 600 and 700 °C, were experimentally determined. Copper, niobium and silicon blocks with the purity of 99.99% (China New Metal Materials Technology Co., Ltd.) were used as starting materials. Sixteen ternary alloys, each with a total mass of usually 1.5 g, were prepared in a non-consumable electrode vacuum arc-melting furnace (WK-I, Physcience Opto-electronics Co., Ltd., Beijing, China) with water-cooled copper crucible under an inert Ar atmosphere. Each alloy was re-melted up to 6 times to improve its homogeneities. During the melting process, a piece of titanium in the center of the crucible was used to capture traces of oxygen. The alloys after arc melting were not subjected to chemical analysis since the mass loss was less than 1 wt.% for all alloys. The button samples were sealed into evacuated quartz tubes with vacuum sealing machine (MRVS−1002, Wuhan Bailibo Technology Co., Ltd., China), annealed at 600 °C (40 d) and 700 °C (30 d) in the high temperature diffusion furnace (KSL−1200X, Hefei Kejing Material Technology Co., Ltd., China), and then quenched into ice water. In order to ensure the rapid cooling of alloy samples, the quartz capsules were broken in the ice water.

After standard metallographic preparation, the microstructure observation and phase identification were carried out by SEM−EDS (acceleration voltage 20 kV, working distance 10 mm) (JSM−6360LV/GENESIS2000XM60, JEOL, Japan) and XRD. The XRD (Smartlab SE, Rigaku corporation, Japan) measurement of the quenched alloys was performed using a Cu K_α radiation at 40 kV and 300 mA. Diffraction patterns were generally

acquired in a scan step of 0.01° over a 2θ range of 20°−90°.

4 Thermodynamic model

The Gibbs energy functions of the pure elements Cu, Nb and Si were taken from the SGTE database compiled by DINSDALE [52]. The thermodynamic parameters for the Cu−Nb, Cu−Si and Si−Nb systems from HÄMÄLÄINEN et al [38], YAN and CHANG [36] and GENG et al [26], respectively, were adopted in the present work. The symbols used to denote the crystallographic data of the phases in the three binary systems are listed in Table 1.

4.1 Solution phases

The solution phases, i.e. liquid, (Cu), hcp(CuSi), bcc(CuSi) and (Nb), were described by the substitutional solution model with the Redlich-Kister-Muggianu polynomial [53,54]. The molar Gibbs energy of the solution phase ϕ is expressed as

$$\begin{aligned} G^{\phi} = & x_{\mathrm{Cu}}{}^{\Theta}G^{\phi}_{\mathrm{Cu}} + x_{\mathrm{Nb}}{}^{\Theta}G^{\phi}_{\mathrm{Nb}} + x_{\mathrm{Si}}{}^{\Theta}G^{\phi}_{\mathrm{Si}} + \\ & RT(x_{\mathrm{Cu}}{}^{\Theta}G^{\phi}_{\mathrm{Cu}} + x_{\mathrm{Nb}}{}^{\Theta}G^{\phi}_{\mathrm{Nb}} + x_{\mathrm{Si}}{}^{\Theta}G^{\phi}_{\mathrm{Si}}) + \\ & x_{\mathrm{Cu}}x_{\mathrm{Nb}}L^{\phi}_{\mathrm{Cu,Nb}} + x_{\mathrm{Cu}}x_{\mathrm{Si}}L^{\phi}_{\mathrm{Cu,Si}} + \\ & x_{\mathrm{Nb}}x_{\mathrm{Si}}L^{\phi}_{\mathrm{Nb,Si}} + x_{\mathrm{Cu}}x_{\mathrm{Nb}}x_{\mathrm{Si}}(x_{\mathrm{Cu}}{}^{0}L^{\phi}_{\mathrm{Cu,Nb,Si}} + \\ & x_{\mathrm{Nb}}{}^{1}L^{\phi}_{\mathrm{Cu,Nb,Si}} + x_{\mathrm{Si}}{}^{2}L^{\phi}_{\mathrm{Cu,Nb,Si}}) \end{aligned} \tag{1}$$

where R represents the molar gas constant, T represents the temperature in K; x_{Cu}, x_{Nb} and x_{Si} represent the molar fractions of the elements Cu, Nb and Si, respectively; ${}^{0}L^{\phi}_{\mathrm{Cu,Nb,Si}}$, ${}^{1}L^{\phi}_{\mathrm{Cu,Nb,Si}}$ and ${}^{2}L^{\phi}_{\mathrm{Cu,Nb,Si}}$ represent the ternary interaction parameters with linearly temperature-dependent to be evaluated.

4.2 Binary phases extending into ternary system

According to the experimental data from the present work, the following binary phases with measured solubilities for the third elements were described by sublattice models [55,56]. For $Cu_{19}Si_6$, $Cu_{15}Si_4$ and $Cu_{56}Si_{11}$, the sublattice models $(Cu,Nb)_{19}Si_6$, $(Cu,Nb)_{15}Si_4$ and $(Cu,Nb)_{56}Si_{11}$ were used in the present work. The bold and underline type mean the normal atoms (i.e., major species). Taking $Cu_{19}Si_6$ as an example, its Gibbs energy can be expressed as

$$\begin{aligned} G^{\mathrm{Cu_{19}Si_6}} = & y'_{\mathrm{Nb}}{}^{\Theta}G^{\mathrm{Cu_{19}Si_6}}_{\mathrm{Nb:Si}} + y'_{\mathrm{Cu}}{}^{\Theta}G^{\mathrm{Cu_{19}Si_6}}_{\mathrm{Cu:Si}} + \\ & 19RT(y'_{\mathrm{Nb}}\ln y'_{\mathrm{Nb}} + y'_{\mathrm{Nb}}\ln y'_{\mathrm{Cu}}) + \\ & y'_{\mathrm{Nb}}y'_{\mathrm{Cu}}[{}^{0}L^{\mathrm{Cu_{19}Si_6}}_{\mathrm{Nb,Cu:Si}} + (y'_{\mathrm{Nb}} - y'_{\mathrm{Cu}}){}^{1}L^{\mathrm{Cu_{19}Si_6}}_{\mathrm{Nb,Cu:Si}} + \cdots] \end{aligned} \tag{2}$$

where y'_{Cu} and y'_{Nb} denote the site fractions of the elements Cu and Nb in the first sublattice. The ternary interaction parameters ${}^{0}L^{\mathrm{Cu_{19}Si_6}}_{\mathrm{Nb,Cu:Si}}$, ${}^{1}L^{\mathrm{Cu_{19}Si_6}}_{\mathrm{Nb,Cu:Si}}$ and ${}^{2}L^{\mathrm{Cu_{19}Si_6}}_{\mathrm{Nb,Cu:Si}}$ are linearly temperature-dependent, which can be expressed as $L^{\mathrm{Cu_{19}Si_6}}_{\mathrm{Nb,Cu:Si}} = A + BT$, and the coefficients A and B will be evaluated in the present work. Analogous expressions are used to describe the Gibbs energies of $Cu_{15}Si_4$, $Cu_{56}Si_{11}$, $NbSi_2$ and Nb_5Si_3_L.

4.3 Ternary compound

The τ_1 phase has the $Nb_5Cu_4Si_4$-type crystal structure with two different atomic sites: 2*a* and 8*h*. Species Nb occupies the sites 2*a*, and species Cu, Si and Nb occupy the sites 8*h*. In view of the experimentally observed negligible homogeneity range, the ternary phase τ_1 is described as stoichiometric compound and its Gibbs energy relative to the pure elements can be formulated by

$$\begin{aligned} {}^{\Theta}G^{\tau_1}_{\mathrm{Cu:Nb:Si}} = & a + bT + 4{}^{\Theta}G^{\mathrm{fcc}}_{\mathrm{Cu}} + \\ & 5{}^{\Theta}G^{\mathrm{bcc}}_{\mathrm{Nb}} + 4{}^{\Theta}G^{\mathrm{diamond}}_{\mathrm{Si}} \end{aligned} \tag{3}$$

where the coefficients a and b are to be optimized in the present work. The parameters ${}^{\Theta}G^{\mathrm{fcc}}_{\mathrm{Cu}}$, ${}^{\Theta}G^{\mathrm{bcc}}_{\mathrm{Nb}}$ and ${}^{\Theta}G^{\mathrm{diamond}}_{\mathrm{Si}}$ are the Gibbs energies of fcc_A1 Cu, bcc_A2 Nb and diamond_A4 Si, respectively.

5 First-principles calculations for enthalpy of formation

The enthalpies of formation at 0 K for all the end-members in the sublattice of the $NbSi_2$, Nb_5Si_3_L and the ternary compound τ_1 as well as τ_2 phases in the Cu–Nb–Si system are computed by means of first-principles calculations to supply reasonable initial values for the thermodynamic parameters for the modeling in the present work. First-principles calculations based on the density functional theory (DFT) [57,58] were performed using the projector augmented wave (PAW) [59,60] pseudo-potentials as implemented in Vienna Ab initio simulation package (VASP) [61,62]. The details of the first-principles calculations can be found in our previous work [63]. The equilibrium

enthalpy of formation, $\Delta H^{eq}(\phi)$ (where ϕ=$NbSi_2$, Nb_5Si_3_L, τ_1 and τ_2) can be expressed as

$$\Delta H^{eq}(\phi) = E(\phi) - [x_{Cu}^{\phi} \cdot E^{eq}(Cu) + x_{Nb}^{\phi} \cdot E^{eq}(Nb) + E^{eq} x_{Si}^{\phi}(Si)] \quad (4)$$

where $E(\phi)$, E^{eq}(Cu), E^{eq}(Nb) and E^{eq}(Si) are equilibrium energies of the compound ϕ and the pure elements Cu, Nb and Si, the reference states are fcc_A1 for Cu, bcc_A2 for Nb, and diamond_A4 for Si, respectively. x_i^{ϕ} is the molar fraction of the component in ϕ phase. The enthalpies of formation at 0 K for τ_1 and τ_2 ternary compounds as well as the end-members of $NbSi_2$ and Nb_5Si_3_L are summarized in Table 3.

Table 3 Enthalpies of formation for $NbSi_2$, Nb_5Si_3, τ_1 and τ_2 phases in Cu−Nb−Si system obtained from first-principles calculations and CALPHAD method

Phase	End-member	ΔH_f/(J·mol^{-1})	
		First-principles calculations, 0 K	CALPHAD, 298.15 K
$NbSi_2$	$NbCu_2$	22342	32477
	$CuNb_2$	19518	25080
	$CuSi_2$	−86171	−
	$SiCu_2$	422366	−
	$SiNb_2$	−31998	−
Nb_5Si_3_L	Nb_5Cu_3	26325	107801
	Cu_5Nb_3	45228	49228
	Cu_5Si_3	22838	−
	Si_5Cu_3	50008	−
	Si_5Nb_3	−8558	−
τ_1	−	−48592	−54909
τ_2	−	−23468	−

6 Results and discussion

6.1 Experimental results and discussion

Sixteen alloys were prepared to determine the phase equilibria of the Cu−Nb−Si system at 600 and 700 °C, respectively. The phases were identified by XRD, and the composition and microstructure were measured by SEM−EDS. Selected microstructures and XRD diffraction patterns of the annealed samples are shown in Figs. 2−5. All the phases in alloys can be easily distinguished based on the contrast of microstructure and chemical composition. The detailed experimental results are summarized in Table 4.

In order to investigate the phase equilibria of the Cu−Nb−Si system at 600 °C, eight alloys of A1−A8 were prepared. Figures 2 and 3 present the BSE images and XRD patterns of the alloys annealed at 600 °C for 40 d, respectively. Figure 2(a) illustrates that Alloy A1 ($Cu_{20}Nb_{15}Si_{65}$) consists of $Cu_{19}Si_6$, (Si) and $NbSi_2$. Figures 2(b) and 3 indicate that Alloy A2 ($Cu_{20}Nb_{40}Si_{40}$) consists of τ_1, Nb_5Si_3 and $NbSi_2$. As presented in Fig. 2(c), τ_1 + $NbSi_2$ + $Cu_{15}Si_4$ exists in Alloy A3. According to Fig. 2(d), Alloy A5 is located in τ_1, $Cu_{56}Si_{11}$ and $Cu_{15}Si_4$ three-phase region, which corresponds well with the XRD results presented in Fig. 3. As illustrated in Fig. 2(e), a three-phase equilibrium of (Cu), τ_1 and Nb_5Si_3 is detected in the Alloy A7 ($Cu_{40}Nb_{35}Si_{25}$). The crystal structures of three phases are identified by XRD, as shown in Fig. 3. Similarly, the Alloy A8 ($Cu_{20}Nb_{65}Si_{15}$) consists of three phases (Cu), (Nb) and Nb_5Si_3_L, as shown in Fig. 2(f), which is supposed by the XRD result in Fig. 3. The solubility of Cu in $NbSi_2$ was measured to be about 3.47 at.% Cu, and that in Nb_5Si_3 was found to be about 8.35 at.% Cu. The determined composition range of the τ_1 phase is 31.93−35.94 at.% Nb, 30.16−33.08 at.% Si, and 30.98−37.91 at.% Cu. Ternary compound τ_2 was not found in this isothermal section at 600 °C.

Alloys A9−A16 were prepared for determining the isothermal section of the Cu–Nb–Si system at 700 °C. Figures 4(a) and 5 show the backscattered electron (BSE) images and XRD patterns for the Alloy A9 ($Cu_{20}Nb_{15}Si_{65}$). According to the SEM−EDS and XRD results, it can be concluded that Alloy A9 is located in the three-phase region, i.e. $Cu_{19}Si_6$ + (Si) + $NbSi_2$. Figures 4(b) and 5 are the BSE micrograph and XRD patterns for the Alloy A10 ($Cu_{20}Nb_{40}Si_{40}$), respectively. According to the SEM−EDS and XRD results, it can be concluded that Alloy A10 is located in the three-phase region of τ_1, Nb_5Si_3_L and $NbSi_2$. Likewise, three phases, i.e. τ_1, $NbSi_2$ and $Cu_{15}Si_4$, coexist in Alloy A11 ($Cu_{40}Nb_{25}Si_{35}$), as shown in Figs. 4(c). Figure 4(d) shows the BSE micrograph for the Alloy A13 ($Cu_{74}Nb_{08}Si_{18}$). The SEM−EDS and XRD analyses indicate that the Alloy A13 is located in a three-phase region, i.e. τ_1, $Cu_{56}Si_{11}$ and $Cu_{15}Si_4$. The Alloy A14 ($Cu_{78}Nb_8Si_{14}$) shows phase region of τ_1 +

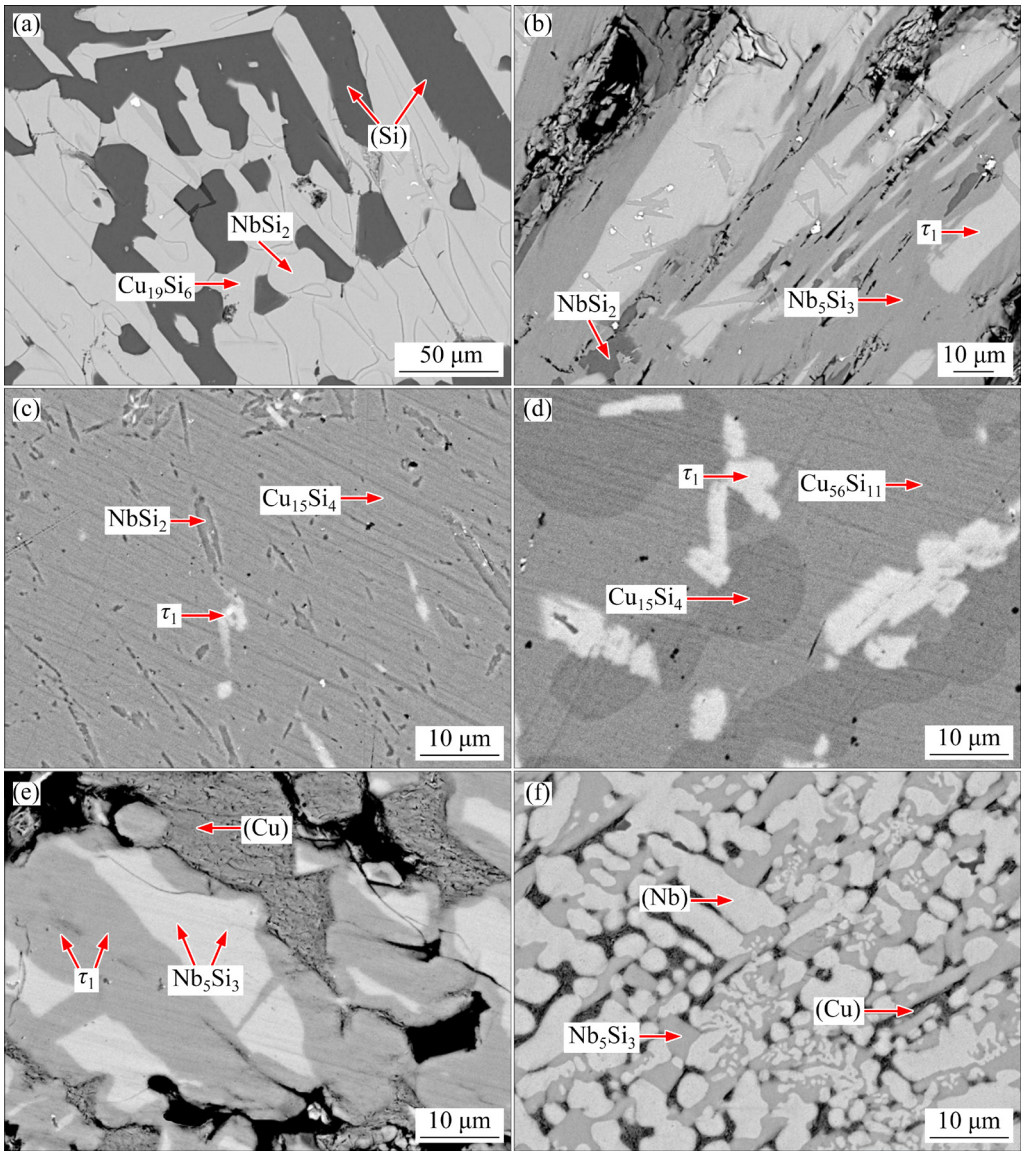

Fig. 2 BSE micrographs of Cu−Nb−Si alloys annealed at 600 °C for 40 d: (a) Alloy A1; (b) Alloy A2; (c) Alloy A3; (d) Alloy A5; (e) Alloy A7; (f) Alloy A8

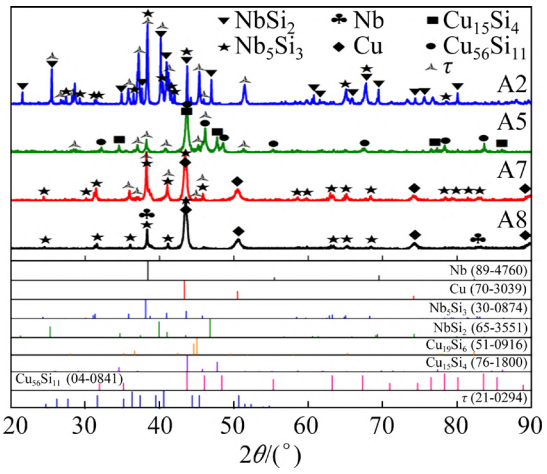

Fig. 3 XRD patterns of Alloys A2, A5 and A7 and A8 in Cu−Nb−Si system annealed at 600 °C for 40 d

hcp(CuSi) + $Cu_{56}Si_{11}$ (see Fig. 4(e)). The BSE micrograph and XRD patterns of the Alloy A16 ($Cu_{40}Nb_{35}Si_{25}$) is shown in Figs. 4(f) and 5, respectively. The SEM−EDS and XRD analysis indicate that the Alloy A16 is located in a three-phase region, i.e. (Cu), (Nb) and Nb_5Si_3_L. The determined maximum solubilities of Cu in the $NbSi_2$ and Nb_5Si_3_L phases at 700 °C are about 4.02 at.% and 8.66 at.%, respectively. The measured composition of the τ_1 phase is 32.0−35.8 at.% Nb, 27.0−33.2 at.% Si and 30.9−39.96 at.% Cu. Ternary compound τ_2 was also not found in the isothermal section at 700 °C.

Based on the analyses of the above experimental results in the present work and the accepted binary

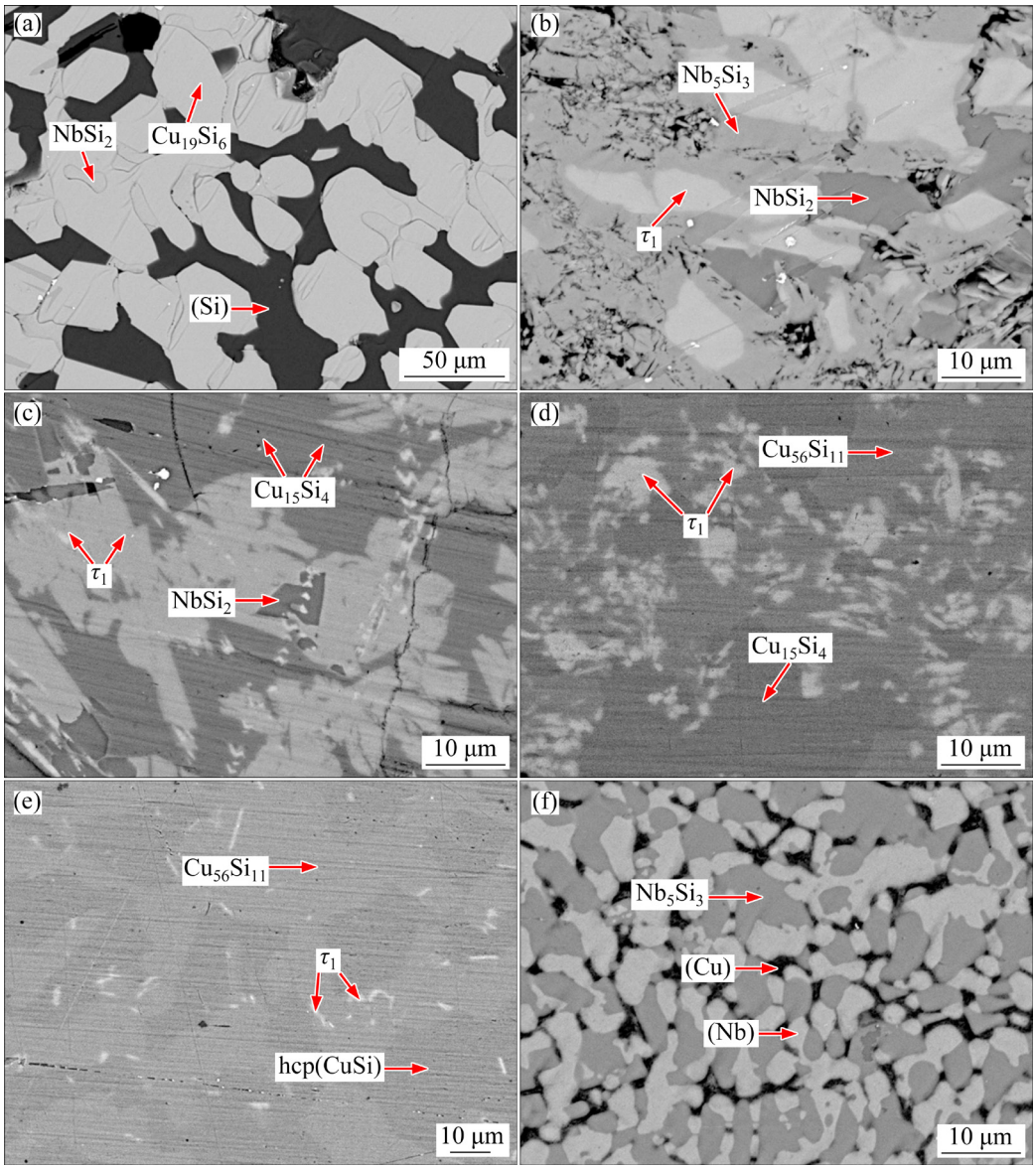

Fig. 4 BSE micrographs of Cu−Nb−Si alloys annealed at 700 °C for 30 d: (a) Alloy A9; (b) Alloy A10; (c) Alloy A11; (d) Alloy A13; (e) Alloy A14; (f) Alloy A16

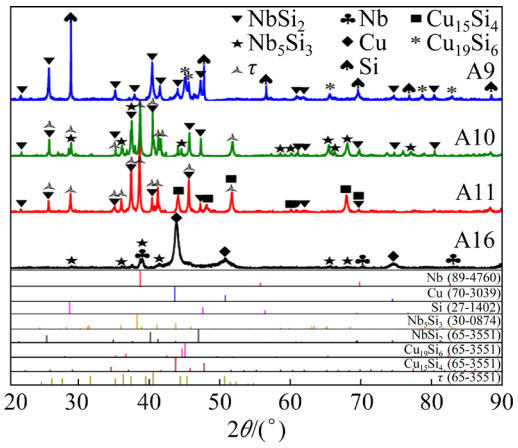

Fig. 5 XRD patterns of Alloys A9, A10, A11 and A16 in Cu−Nb−Si system annealed at 700 °C for 30 d

phase diagrams, the isothermal sections of the Cu−Nb−Si system at 600 and 700 °C were constructed, as shown in Figs. 6(a) and (b), respectively. It can be seen that the phase equilibria of the Cu−Nb−Si system at 600 and 700 °C are similar. For the isothermal section at 600 °C, seven three-phase regions, (Si) + $Cu_{19}Si_6$ + $NbSi_2$, $NbSi_2$ + Nb_5Si_3_L + τ_1, $NbSi_2$ + $Cu_{15}Si_4$ + τ_1, $Cu_{15}Si_4$ + $Cu_{19}Si_6$ + $NbSi_2$, $Cu_{15}Si_4$+$Cu_{56}Si_{11}$ + τ_1, (Cu) + Nb_5Si_3_L + τ_1, and (Cu) + Nb_5Si_3_L + (Nb), and a two-phase regions τ_1 + hcp(CuSi), were measured. Two three-phase regions hcp(CuSi) + $Cu_{56}Si_{11}$ + τ_1 and hcp(CuSi) + (Cu) + τ_1 were extrapolated based on the Gibbs phase rule and the phase regions of Alloys A5−A7.

Table 4 Phases and compositions determined by XRD and SEM−EDS of Cu−Nb−Si alloys annealed at 600 and 700 °C

Alloy No.	Nominal composition/at.%	Annealed temperature/°C	Annealed time/d	Phase identified	Phase composition/at.%		
					Cu	Nb	Si
A1	$Cu_{20}Nb_{15}Si_{65}$	600	40	(Si)	0.03	2.99	96.98
	$Cu_{20}Nb_{15}Si_{65}$	600	40	$NbSi_2$	0.96	35.98	63.06
	$Cu_{20}Nb_{15}Si_{65}$	600	40	$Cu_{19}Si_6$	75.36	0.54	24.1
A2	$Cu_{20}Nb_{40}Si_{40}$	600	40	$NbSi_2$	1.07	37.36	61.57
	$Cu_{20}Nb_{40}Si_{40}$	600	40	Nb_5Si_3_L	2	60.88	37.12
	$Cu_{20}Nb_{40}Si_{40}$	600	40	τ_1	30.98	35.94	33.08
A3	$Cu_{40}Nb_{25}Si_{35}$	600	40	$NbSi_2$	3.46	36.2	60.34
	$Cu_{40}Nb_{25}Si_{35}$	600	40	τ_1	33.96	34	32.04
	$Cu_{40}Nb_{25}Si_{35}$	600	40	$Cu_{15}Si_4$	78.56	0.4	21.04
A4	$Cu_{72}Nb_3Si_{25}$	600	40	$NbSi_2$	3.47	35.45	61.08
	$Cu_{72}Nb_3Si_{25}$	600	40	$Cu_{19}Si_6$	75.1	0.56	24.34
	$Cu_{72}Nb_3Si_{25}$	600	40	$Cu_{15}Si_4$	78.55	0.25	21.2
A5	$Cu_{78}Nb_3Si_{19}$	600	40	τ_1	37.91	31.93	30.16
	$Cu_{78}Nb_3Si_{19}$	600	40	$Cu_{15}Si_4$	78.49	0.47	21.04
	$Cu_{78}Nb_3Si_{19}$	600	40	$Cu_{56}Si_{11}$	83.2	0.17	16.63
A6	$Cu_{84}Nb_3Si_{13}$	600	40	τ_1	37.07	32.98	29.95
	$Cu_{84}Nb_3Si_{13}$	600	40	hcp(CuSi)	87.86	0.11	12.03
A7	$Cu_{40}Nb_{35}Si_{25}$	600	40	τ_1	35.71	34.25	30.04
	$Cu_{40}Nb_{35}Si_{25}$	600	40	(Cu)	94.13	3.01	2.86
	$Cu_{40}Nb_{35}Si_{25}$	600	40	Nb_5Si_3_L	5.84	61.12	33.04
A8	$Cu_{20}Nb_{65}Si_{15}$	600	40	(Cu)	96.07	3.07	0.86
	$Cu_{20}Nb_{65}Si_{15}$	600	40	(Nb)	3.09	95.88	1.03
	$Cu_{20}Nb_{65}Si_{15}$	600	40	Nb_5Si_3_L	8.35	62.25	29.4
A9	$Cu_{20}Nb_{15}Si_{65}$	700	30	(Si)	1.8	2.25	95.95
	$Cu_{20}Nb_{15}Si_{65}$	700	30	$NbSi_2$	2.04	35.11	62.85
	$Cu_{20}Nb_{15}Si_{65}$	700	30	$Cu_{19}Si_6$	74.52	0.66	24.82
A10	$Cu_{20}Nb_{40}Si_{40}$	700	30	$NbSi_2$	2.03	37.17	60.8
	$Cu_{20}Nb_{40}Si_{40}$	700	30	Nb_5Si_3_L	2.08	61	36.92
	$Cu_{20}Nb_{40}Si_{40}$	700	30	τ_1	30.93	35.83	33.24
A11	$Cu_{40}Nb_{25}Si_{35}$	700	30	$NbSi_2$	3.47	35.85	60.68
	$Cu_{40}Nb_{25}Si_{35}$	700	30	τ_1	33.04	34.65	32.31
	$Cu_{40}Nb_{25}Si_{35}$	700	30	$Cu_{15}Si_4$	78.14	0.83	21.03
A12	$Cu_{62}Nb_{03}Si_{25}$	700	30	$NbSi_2$	4.02	34.92	61.06
	$Cu_{62}Nb_{03}Si_{25}$	700	30	$Cu_{19}Si_6$	74.71	0.85	24.44
	$Cu_{62}Nb_{03}Si_{25}$	700	30	$Cu_{15}Si_4$	78.18	0.28	21.54
A13	$Cu_{77}Nb_{03}Si_{20}$	700	30	τ_1	37.99	31.92	30.09
	$Cu_{77}Nb_{03}Si_{20}$	700	30	$Cu_{15}Si_4$	78.39	0.98	20.63
	$Cu_{77}Nb_{03}Si_{20}$	700	30	$Cu_{56}Si_{11}$	82.41	0.55	17.04
A14	$Cu_{72}Nb_3Si_{15}$	700	30	τ_1	40.01	31.96	28.03
	$Cu_{72}Nb_3Si_{15}$	700	30	hcp(CuSi)	86.65	0.36	12.99
	$Cu_{72}Nb_3Si_{15}$	700	30	$Cu_{56}Si_{11}$	82.79	0.74	16.47
A15	$Cu_{40}Nb_{35}Si_{25}$	700	30	τ_1	34.66	36.22	29.12
	$Cu_{40}Nb_{35}Si_{25}$	700	30	(Cu)	90.83	4.74	4.43
	$Cu_{40}Nb_{35}Si_{25}$	700	30	Nb_5Si_3_L	5.08	61.13	33.79
A16	$Cu_{20}Nb_{65}Si_{15}$	700	30	(Cu)	94.84	4.02	1.14
	$Cu_{20}Nb_{65}Si_{15}$	700	30	(Nb)	3.98	92.72	3.3
	$Cu_{20}Nb_{65}Si_{15}$	700	30	Nb_5Si_3_L	8.66	62.07	29.27

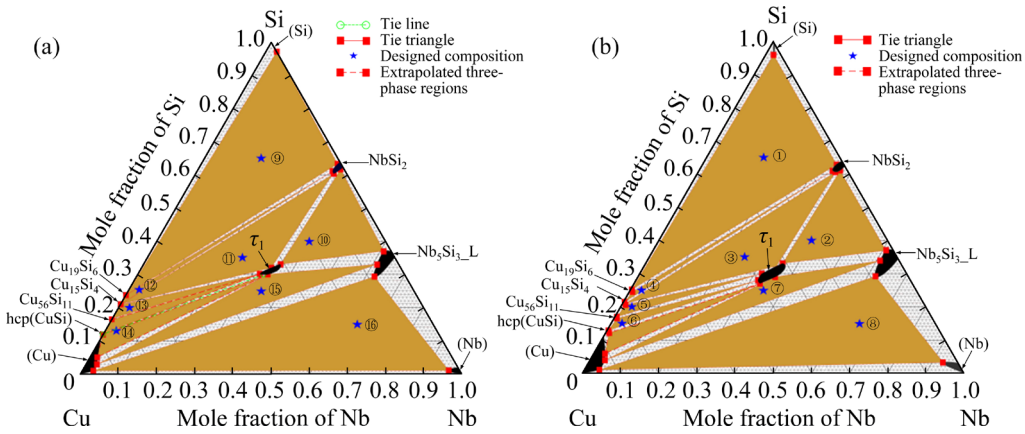

Fig. 6 Constructed isothermal sections of Cu−Nb−Si system at 600 °C (a) and 700 °C (b)

For the isothermal section at 700 °C, eight three-phase regions, (Si) + $Cu_{19}Si_6$ + $NbSi_2$, $NbSi_2$ + Nb_5Si_3_L + τ_1, $NbSi_2$ + $Cu_{15}Si_4$ + τ_1, $Cu_{15}Si_4$ + $Cu_{19}Si_6$ + $NbSi_2$, $Cu_{15}Si_4$ + $Cu_{56}Si_{11}$ + τ_1, hcp(CuSi) + $Cu_{56}Si_{11}$ + τ_1, (Cu) + Nb_5Si_3_L + τ_1, and (Cu) + Nb_5Si_3_L + (Nb), were determined. According to the Gibbs phase rule and the phase regions of Alloys A14 and A15, a three-phase region hcp(CuSi) + (Cu) + τ_1 was extrapolated.

EDS analyses indicated that the solubilities of Cu in the (Nb) phase are about 3.09 and 3.98 at.% at 600 and 700 °C, respectively. Besides, the measured maximum solubilities of Cu in the $NbSi_2$ phase are about 4.02 and 3.47 at.% at 600 and 700 °C, respectively, and those of the measured maximum solubilities of Cu in the Nb_5Si_3_L phase are about 8.35 and 8.66 at.% at 600 and 700 °C, respectively. According to the EDS results listed in Table 4, the homogeneity range of τ_1 phase is 32.0−35.8 at.% Nb, 27.0−33.2 at.% Si and 30.9−39.96 at.% Cu. The solubilities of Nb in the $Cu_{19}Si_6$, $Cu_{15}Si_4$, $Cu_{56}Si_{11}$, and hcp(CuSi) phase are measured to be less than 1 at.%.

6.2 Thermodynamic calculation results and discussion

Based on the experimental data available in the present work and literature, the Cu−Nb−Si system was evaluated by the optimization module PARROT [64] of the program Thermo-Calc software, which works by minimizing the square sum of the differences between measured and calculated values. In the first step, the enthalpies of formation at 0 K for the end-members of the $NbSi_2$, Nb_5Si_3, as well as τ_1 phases calculated by first-principles were used as the reasonable initial values. Then, the data of three-phase region of the isothermal sections at 600 and 700 °C were considered one by one in the optimization process. Finally, all parameters were optimized simultaneously to achieve a self-consistent thermodynamic description. The obtained thermodynamic parameters of the Cu−Nb−Si system are listed in Table 5.

The enthalpies of formation for the end-members of the $NbSi_2$, Nb_5Si_3_L and the ternary compound τ_1 as well as τ_2 phases computed by the first-principles calculations compared with the CALPHAD approach are summarized in Table 3. As shown in Table 3, most of the enthalpies of formation for the end-members by using the first-principles calculations and CALPHAD approach are in reasonable agreement except for the end-members Nb_5Cu_3. In order to reproduce the three-phase regions (Cu) + Nb_5Si_3_L + (Nb) and (Cu) + Nb_5Si_3_L + τ_1, as well as the solubility of Nb_5Si_3_L, the enthalpy of formation for the end-members Nb_5Cu_3 should be more positive than those calculated by the first-principles calculations.

Figures 7(a) and (b) show the calculated isothermal sections at 600 and 700 °C of the Cu−Nb−Si system in comparison with the experimental data from the present work, respectively. It is found that the isothermal sections at 600 and 700 °C contain nine three-phase regions, i.e., (Si) + $Cu_{19}Si_6$ + $NbSi_2$, $NbSi_2$ + Nb_5Si_3_L + τ_1, $NbSi_2$ + $Cu_{15}Si_4$ + τ_1, $Cu_{15}Si_4$ + $Cu_{19}Si_6$ + $NbSi_2$, $Cu_{15}Si_4$+$Cu_{56}Si_{11}$ + τ_1, hcp(CuSi) + $Cu_{56}Si_{11}$ + τ_1, (Cu) + Nb_5Si_3_L + τ_1, hcp(CuSi) + (Cu) + τ_1, and (Cu) + Nb_5Si_3_L + (Nb).

Table 5 Obtained thermodynamic parameters of Cu−Nb−Si system in present work

Phase	Model	Thermodynamic parameter[a]
$Cu_{15}Si_4$	$(Cu,Nb)_{15/19}(Si)_{4/19}$	${}^{\Theta}G^{Cu_{15}Si_4}_{Nb,Si} = 90000 + (15/19){}^{\Theta}G^{Cu_{15}Si_4}_{Nb} + (4/19){}^{\Theta}G^{Cu_{15}Si_4}_{Si}$, ${}^{\Theta}G^{Cu_{15}Si_4}_{Cu,Nb:Si} = -18897$
$Cu_{19}Si_6$	$(Cu,Nb)_{19/25}(Si)_{6/25}$	${}^{\Theta}G^{Cu_{19}Si_6}_{Nb:Si} = 5000 + (19/25){}^{\Theta}G^{Cu_{19}Si_6}_{Nb} + (6/25){}^{\Theta}G^{Cu_{19}Si_6}_{Si}$, ${}^{\Theta}G^{Cu_{19}Si_6}_{Cu,Nb:Si} = -18758$
$Cu_{56}Si_{11}$	$(Cu,Nb)_{56/67}(Si)_{11/67}$	${}^{\Theta}G^{Cu_{56}Si_{11}}_{Nb:Si} = 117620 + (56/67){}^{\Theta}G^{Cu_{56}Si_{11}}_{Cu} + (11/67){}^{\Theta}G^{Cu_{56}Si_{11}}_{Si}$, ${}^{\Theta}G^{Cu_{56}Si_{11}}_{Cu,Nb:Si} = -8843$
$Nb_5Si_3\_L$	$(Cu,Nb,Si)_{0.625}(Cu,Nb,Si)_{0.375}$	${}^{\Theta}G^{Nb_5Si_3\_L}_{Nb:Cu} = 107801 + 0.625{}^{\Theta}G^{Nb_5Si_3\_L}_{Nb} + 0.375{}^{\Theta}G^{Nb_5Si_3\_L}_{Cu}$, ${}^{\Theta}G^{Nb_5Si_3\_L}_{Nb:Cu} = 49228 + 0.625{}^{\Theta}G^{Nb_5Si_3\_L}_{Cu} + 0.375{}^{\Theta}G^{Nb_5Si_3\_L}_{Nb}$, ${}^{\Theta}G^{Nb_5Si_3\_L}_{Nb:Cu,Si} = -385487.03 - 5.78T$
$NbSi_2$	$(Cu,Nb,Si)_{0.333333}(Cu,Nb,Si)_{0.66667}$	${}^{\Theta}G^{NbSi_2}_{Cu:Cu} = 5000 + {}^{\Theta}G^{NbSi_2}_{Cu}$, ${}^{\Theta}G^{NbSi_2}_{Nb:Nb} = 5000 + {}^{\Theta}G^{NbSi_2}_{Nb}$, ${}^{\Theta}G^{NbSi_2}_{Nb:Cu} = 32477 + (1/3){}^{\Theta}G^{NbSi_2}_{Nb} + (2/3){}^{\Theta}G^{NbSi_2}_{Cu}$, ${}^{\Theta}G^{NbSi_2}_{Cu:Nb} = 25080 + (1/3){}^{\Theta}G^{NbSi_2}_{Cu} + (2/3){}^{\Theta}G^{NbSi_2}_{Nb}$, ${}^{\Theta}G^{NbSi_2}_{Nb:Cu,Si} = -74536$
τ_1	$(Cu)_{5/14}(Nb)_{5/14}(Si)_{5/14}$	${}^{\Theta}G^{\tau_1}_{Cu:Nb:Si} = -54909 - 4.615T + (4/13){}^{\Theta}G^{\tau_1}_{Cu} + (5/13){}^{\Theta}G^{\tau_1}_{Nb} + (4/13){}^{\Theta}G^{\tau_1}_{Si}$

[a] Temperature (T) in K, and Gibbs energy in J/mol

The Gibbs energies for the pure elements were derived from the compilation of DINSDALE [52]. The thermodynamic parameters for the Cu−Nb, Cu−Si and Nb−Si systems from HÄMÄLÄINEN et al [38], YAN and CHANG [36], and GENG et al [26], respectively, were adopted in the present work

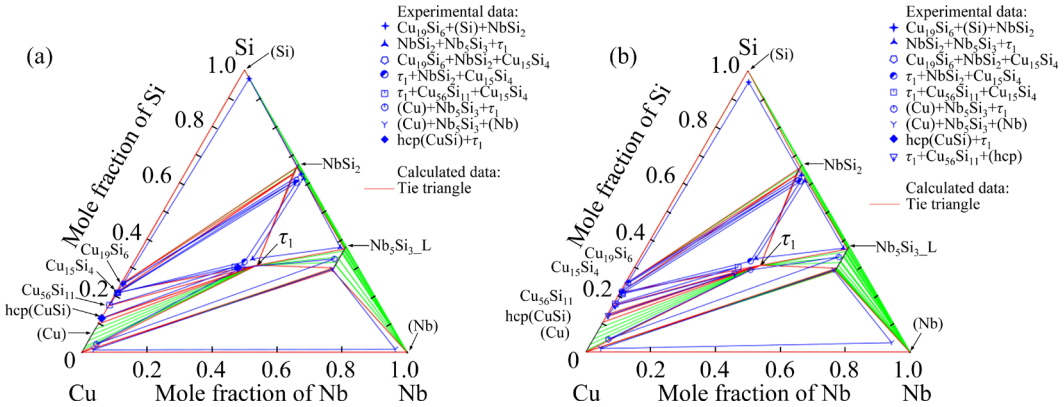

Fig. 7 Calculated isothermal sections of Cu−Nb−Si system at 600 °C (a) and 700 °C (b) along with experimental data from present work

As can be seen from these calculated isothermal sections, most of the calculated data show a reasonable agreement with the measured ones except some data points in the Nb- and Cu-rich corners. The calculated solubilities of Cu and Si in the (Nb) phase, and Nb and Si in the (Cu) phase are noticeably smaller than the measured one. In the calculated Cu−Nb and Si−Nb phase diagrams (see Fig. 1), the solubilities of Cu and Si in the (Nb) phase are small below 600 °C. It makes the

calculated solubility of the (Nb) phase lower than the experimental one. Likewise, the same reason can be elucidated for the discrepancy of solubilities in the Cu-rich corner. The calculated solubilities of Cu in the Nb_5Si_3_L phase are about 8.51 and 8.57 at.%, at 600 and 700 °C, respectively, showing a reasonable agreement with the measured values of 8.35 and 8.66 at.%. The calculated solubilities of Cu in the $NbSi_2$ phase are about 3.66 and 3.97 at.% at 600 and 700 °C, respectively, which are consistent with the experimental results of 3.47 and 4.02 at.%. The calculated solubilities of Nb in $Cu_{19}Si_6$, $Cu_{15}Si_4$, $Cu_{56}Si_{11}$, and hcp(CuSi) are all less than 1 at.%, which are consistent with experimental data. In Fig. 8, calculated isothermal section at 800 °C of the Cu−Nb−Si system is compared with the observed ones by SAVITSKII et al [20] and ZANKL and MALTER [21]. It can be seen in Fig. 8(a) that nine three-phase regions, i.e., (Si) + $Cu_{19}Si_6$ + $NbSi_2$, $NbSi_2$ + Nb_5Si_3_L + τ_1, τ_1 + $Cu_{19}Si_6$ + $NbSi_2$, $Cu_{33}Si_7$ + $Cu_{19}Si_6$ + $NbSi_2$, $Cu_{33}Si_7$ + bcc(CuSi) + τ_1, hcp(CuSi) + bcc(CuSi) + τ_1, (Cu) + Nb_5Si_3_L + τ_1, hcp(CuSi) + (Cu) + τ_1, and (Cu) + Nb_5Si_3_L + (Nb) were calculated. However, the present calculated phase relations are not consistent with the experimental data [20,21]. These discrepancies can be interpreted by the following two reasons. On the one hand, according to the present experimental results, as the temperature increases, the Nb_5Si_3_L phase extends more into the three-phase region, and the three-phase region (Cu) + Nb_5Si_3_L + (Nb) will be more stable, which may not be replaced by the three-phase region (Cu) + τ_1 + (Nb). The samples may not diffuse completely even after 200 h of annealing at 800 °C. Thus, the reported three-phase region (Cu) + τ_1 + (Nb) seemed to be questionable [20]. On the other hand, ZANKL and MALTER [21] did not detect the hcp(CuSi), bcc(CuSi), $Cu_{33}Si_7$ and τ_1 phases in their experiments. The experimental results [21] are inconsistent with the accepted Cu−Si binary phase diagram in Fig. 1(b). We surmise that the samples were annealed at 800 °C for only 20 h without reaching phase equilibrium condition [21]. Based on the above discussions, the data from SAVITSKII et al [20] and ZANKL and MALTER [21] were not used during the thermodynamic optimization.

7 Conclusions

(1) The phase equilibria of the Cu−Nb−Si system at 600 and 700 °C were investigated by XRD and SEM−EDS. According to the experimental results, two isothermal sections were constructed. Ternary compound τ_1 ($Cu_4Nb_5Si_4$) was confirmed to exist in the Cu−Nb−Si ternary system at 600 and 700 °C.

(2) The first-principles calculations were performed to compute the enthalpies of formation at 0 K for the end-members of the $NbSi_2$, Nb_5Si_3_L and the ternary compound τ_1 as well as τ_2 phases to provide reasonable initial values.

(3) The measured maximum solubilities of Cu in Nb_5Si_3_L and $NbSi_2$ at 700 °C are about 8.66 and 4.02 at.%, respectively. At 600 °C, the maximum solubilities of Cu in Nb_5Si_3_L and $NbSi_2$ are about 8.35 and 3.47 at.%, respectively. The homogeneity range of τ_1 phase is 32.0−35.8 at.% Nb, 27.0−33.2 at.% Si and 30.9−39.96 at.% Cu. The measured solubilities of Nb in $Cu_{19}Si_6$,

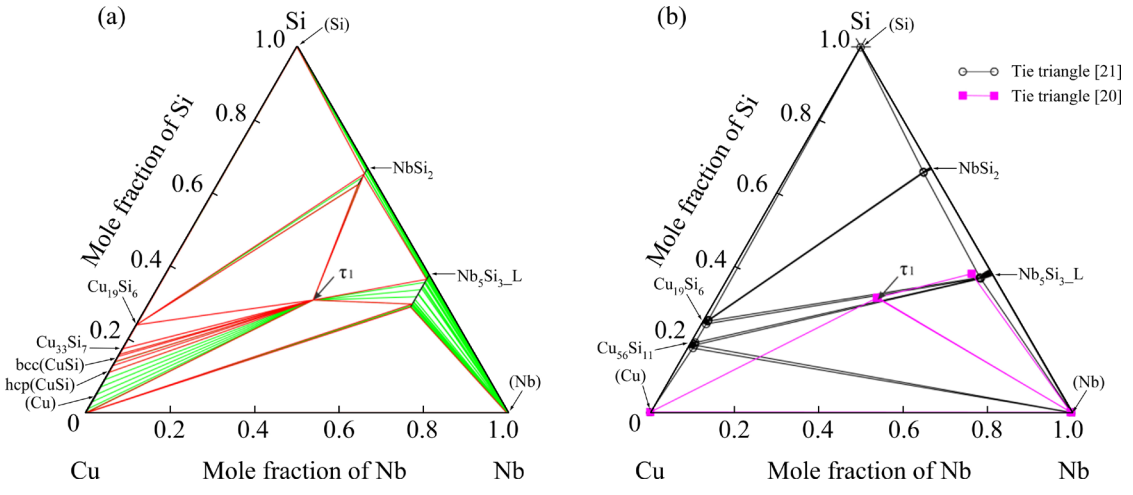

Fig. 8 Calculated (a) and observed (b) isothermal sections of Cu−Nb−Si system at 800 °C

$Cu_{15}Si_4$, $Cu_{56}Si_{11}$, and hcp(CuSi) are all less than 1 at.%.

(4) The thermodynamic assessment of the Cu−Nb−Si system was carried out by using the CALPHAD method based on the experimental data available in the present work and literature. A set of self-consistent thermodynamic parameters of the Cu−Nb−Si systems was obtained. The present thermodynamic parameters can reproduce most of the reliable experimental data.

Acknowledgments

The work was supported by the National Natural Science Foundation of China (No. 52071002), the National Natural Science Foundation of Anhui Province, China (No. 2008085QE200), and the Major Science and Technology Project of Precious Metal Materials Genetic Engineering in Yunnan Province, China (Nos. 2019ZE001-1, 202002AB080001).

References

[1] YI Jiang, JIA Yan-lin, ZHAO Yu-yuan, XIAO Zhu, HE Ke-jian, WANG Qi, WANG Ming-pu, LI Zhou. Precipitation behavior of Cu−3.0Ni−0.72Si alloy [J]. Acta Materialia, 2019, 166: 261−270.

[2] XIAO Meng , DU Yong, LIU Zhi-jian, XU Kai, CHEN Chong, QIU Lian-chang, ZHANG Hua-qing, LIU Yu-ling, LIU Shu-hong. Phase equilibria of the Cu−Zr−Si system at 750 and 900 °C [J]. Calphad, 2020, 68: 101727.

[3] WANG Jian, ZHANG Hong-tao, FU Hua-dong, XIE Jian-xin. Effect of Cr content on microstructure and properties of aged Cu−Cr−P alloys [J]. Transactions of Nonferrous Metals Society of China, 2021, 31(1): 232−242.

[4] WANG Xu, LI Zhou, XIAO Zhu, QIU Wen-ting. Microstructure evolution and hot deformation behavior of Cu−3Ti−0.1Zr alloy with ultra-high strength [J]. Transactions of Nonferrous Metals Society of China, 2020, 30(10): 2737−2748.

[5] ZHAO Chao, WANG Zhi, PAN De-qing, LI Dao-xi, LUO Zong-qiang, ZHANG Da-tong, YANG Chao, ZHANG Wei-wen. Effect of Si and Ti on dynamic recrystallization of high-performance Cu−15Ni−8Sn alloy during hot deformation [J]. Transactions of Nonferrous Metals Society of China, 2019, 29(12): 2556−2565.

[6] KOMARASAMY M, LI X, WHALEN S A, MA X L, CANFIELD N, OLSZTA M J, VARGA T, SCHEMER-KOHRN A L, YU A Q, OVERMAN N R, MATHAUDHU S N, GRANT G J. Microstructural evolution in Cu−Nb processed via friction consolidation [J]. Journal of Materials Science and Technology, 2021, 56(22): 12864−12880.

[7] TSCHOPP M A, MURDOCH H A, KECSKES L J, DARLING K A. “Bulk” nanocrystalline metals: Review of the current state of the art and future opportunities for copper and copper alloys [J]. JOM, 2014, 66(6): 1000−1019.

[8] MA Rui, GUO Xi-ping. Influence of molybdenum contents on the microstructure, mechanical properties and oxidation behavior of multi-elemental Nb−Si based ultrahigh temperature alloys [J]. Intermetallics, 2021, 129: 107053.

[9] SUN Guang-xin, JIA Li-na, YE Cheng-tong, JIN Zu-heng, WANG Yu, LI Hang, ZHANG Hu. Balancing the fracture toughness and tensile strength by multiple additions of Zr and Y in Nb−Si based alloys [J]. Intermetallics, 2021, 133: 107172.

[10] KARTAVYKH A V, KALOSHKIN S D, CHERDYNTSEV V V, GORSHENKOV M V, SVIRIDOVA T A, BORISOVA Y V, SENATOV F S, MAKSIMKIN A V. Application of microstructured intermetallides in turbine manufacture. Part 1: Present state and prospects (a review) [J]. Inorganic Materials: Applied Research, 2013, 4 (1): 12−20.

[11] HU Biao, DU Yong, LIU Shu-hong, LIU Yu-ling, HUANG Lei, SHI Chen-ying. A new thermodynamic database for multicomponent Cu alloys [J]. Calphad, 2019, 67: 101618.

[12] QIU Cheng-liang, HU Biao, ZHOU Jia-qiang, WU Pei-lu, LIU Yin, WANG Cheng-jun, DU Yong. The phase equilibria of the Cu–Cr–Ni and Cu–Cr–Ag systems: Experimental investigation and thermodynamic modeling [J]. Calphad, 2020, 68: 101734.

[13] QIU Cheng-liang, HU Biao, ZHANG Yu, WANG Xiu-yu, WANG Qing-ping, MIN Fan-fei, DU Yong. Experimental investigation and thermodynamic modeling of the Cu–Ag–Si ternary system [J]. The Journal of Chemical Thermodynamics, 2020, 150: 106172.

[14] ZHOU Jia-qiang, HU Biao, SHI Yu-chao, WANG Qing-ping, WANG Cheng-jun, DU Yong. Experimental investigation and thermodynamic modeling of the phase equilibria in the Cu−Nb−Ni ternary system [J]. Journal of Phase Equilibria and Diffusion, 2021, 42(1): 150−163.

[15] DREVAL L, ZENG Yin-ping, DOVBENKO O, DU Yong, LIU Shu-hong, HU Biao, ZHANG Hua-qing. Thermodynamic description and simulation of solidification microstructures in the Cu−Mg−Zn system [J]. Journal of Materials Science and Technology, 2021, 56: 10614−10639.

[16] ZHANG Yu, HU Biao, LI Ben-fu, ZHANG Man, WANG Qing-ping, DU Yong. Experimental investigation and CALPHAD modeling of the Cu−Cr−Si ternary system [J]. Calphad, 2021, 74: 102324.

[17] LUKAS H L, FRIES S G, SUNDMAN B. Computational thermodynamics: The CALPHAD method [M]. Cambridge: Cambridge University Press, 2007.

[18] LIU Zi-kui, WANG Yi. Computational thermodynamics of materials [M]. Cambridge: Cambridge University Press, 2016.

[19] GANGLBERGER E. The crystal structure of $Nb_5Cu_4Si_4$ [J]. Monatshefte Für Chemie, 1968, 99: 549−556. (in German)

[20] SAVITSKII E M, EFIMOV Y V, FROLOVA T M. Copper effect on structure and superconductive properties of transition metal silicides [J]. Neorganicheskie Materialy, 1979, 15(4): 512−515.

[21] ZANKL R, MALTER R. Phase equilibria in the system copper–niobium–silicon [J]. Zeitschrift Für Metallkunde, 1981, 72(10): 720−724.

[22] PAN V M, LATYSHEVA V I, KULIK O G, POPOV A G. Influence of alloying with germanium and copper on the conditions of formation of the superconducting compound Nb_3Si [J]. Russian Metallurgy, 1982, 3: 167−171.

[23] VILLARS P, CALVERT L D. Pearson's handbook of crystallographic data [M]. Materials Park: American Society for Metals, 1991.

[24] OLESINSKI R W, ABBASCHIAN G J. The Cu−Si (copper–silicon) system [J]. Bulletin of Alloy Phase Diagrams, 1986, 7: 170−178.

[25] GENG Tai, LI Chang-rong, BAO Jing, ZHAO Xing-qing, DU Zhen-min, GUO Cui-ping. Thermodynamic assessment of the Nb−Si−Ti system [J]. Intermetallics, 2009, 17: 343−357.

[26] GENG Tai, LI Chang-rong, ZHAO Xing-qing, XU Hui-bin, DU Zhen-min, GUO Cui-ping. Thermodynamic assessment of the Nb−Si−Mo system [J]. Calphad, 2010, 34: 363−376.

[27] FUJIO S, TANAKA K, INUI H. Formation probability for enantiomorphic crystals (with the space groups of *P*6222 and *P*6422) in transition-metal disilicides with the C40 structure as determined by convergent-beam electron diffraction [J]. Intermetallics, 2007, 15(3): 245−252.

[28] MORRAL F R, WESTGREN A. The crystal structure of a complex copper−silicon compound [J]. Arkiv foer Kemi, Mineralogi och Geologi, 1934, 11B: 1−6.

[29] SOLBERG K J. The crystal structure of η-Cu_3Si precipitates in silicon [J]. Acta Crystallographica A, 1978, 34: 684−698.

[30] MUKHERJEE K P, BANDYOPADHYAYA J, GUPTA K P. Phase relationship and crystal structure of intermediate phases in the Cu−Si system in the composition range 17 to 25 at. pct Si [J]. Transaction of American Institute of Mining, Metallurgical, and Petroleum Engineers (AIME), 1969, 245: 2335−2338.

[31] SHIN D, SAAL J E, LIU Zi-kui. Thermodynamic modeling of the Cu−Si system [J]. Calphad, 2008, 32: 520−526.

[32] JACOBS M, BÜHLER T. System Cu−Si, in: COST 507: thermochemical database for light metal alloys [J]. European Communities, 1998, 2: 178−181.

[33] GIERLOTKA W, AZIZUL HAQUE M. On the binary (Cu + Si) system: Thermodynamic modelling of the phase diagram and atomic mobility in face centred cubic phase [J]. The Journal of Chemical Thermodynamics, 2013, 57: 32−38.

[34] HALLSTEDT B, GRÖBNER J, HAMPL M, SCHMID-FETZER R. Calorimetric measurements and assessment of the binary Cu−Si and ternary Al−Cu−Si phase diagrams [J]. Calphad, 2016, 53: 25−38.

[35] SUFRYD K, PONWEISER N, RIANI P, RICHTER K W, CACCIAMANI G. Experimental investigation of the Cu−Si phase diagram at x(Cu)>0.72 [J]. Intermetallics, 2011, 19: 1479−1488.

[36] YAN X Y, CHANG Y A. A thermodynamic analysis of the Cu−Si system [J]. Journal of Alloys and Compounds, 2000, 308: 221−229.

[37] DU Yong, LIU Shu-hong, ZHANG Li-jun, XU Hong-hui, ZHAO Dong-dong, WANG Ai-jun, ZHOU Liang-cai. An overview on phase equilibria and thermodynamic modeling in multicomponent Al alloys: Focusing on the Al−Cu−Fe−Mg–Mn−Ni−Si−Zn system [J]. Calphad, 2011, 35(3): 427−445.

[38] HÄMÄLÄINEN M, JÄÄSKELÄINEN K, LUOMA R, NUOTIO M, TASKINEN P, TEPPO O. A thermodynamic analysis of the binary alloy systems Cu−Cr, Cu−Nb and Cu−V [J]. Calphad, 1990, 14(2): 125−137.

[39] FERNANDES P B, COELHO G C, FERREIRA F, NUNES C A, SUNDMAN B. Thermodynamic modeling of the Nb−Si system [J]. Intermetallics, 2002, 10: 993−999.

[40] YANG Y, CHANG Y A, ZHAO J C, BEWLAY B P. Thermodynamic modeling of the Nb−Hf−Si ternary system [J]. Intermetallics, 2003, 11: 407−415.

[41] SHAO G. Thermodynamic assessment of the Nb−Si−Al system [J]. Intermetallics, 2004, 12: 655−664.

[42] DAVID N, CARTIGNY Y, BELMONTE T, FIORANI J M, VILASI M. Thermodynamic description of the Cr−Nb−Si isothermal section at 1473 K [J]. Intermetallics, 2006, 14: 464−473.

[43] POPOV I A, SHIRYAEVA N V. Equilibrium diagram of the Cu−Nb system [J]. Russian Journal of Inorganic Chemistry, 1961, 6: 1184−1187.

[44] VERHOEVEN J D, GIBSON E D. The monotectic reaction in Cu−Nb alloys [J]. Journal of Materials Science, 1978, 13: 1576−1582.

[45] TEREKHOV G I, ALEXANDROVA L N. Phase equilibria Cu−Nb [J]. Izvestiya Akademii Nauk SSSR, Metally, 1984, 4: 210−213. (in Russian)

[46] OKAMOTO H. Cu−Nb (copper−niobium) [J]. Journal of Phase Equilibria and Diffusion, 1991, 12: 614−615.

[47] SMITH J F, LEE K J, BAILEY D M. Resolution of conflicting data: I. Temperature and equilibrium [J]. Bulletin of Alloy Phase Diagrams, 1984, 5(2): 133−134.

[48] CHAKRABARTI D J, LAUGHLIN D E. "Cu−Nb (copper−niobium)" phase diagrams of binary copper alloys [M]. Materials Park: American Society for Metals International, 1994.

[49] LI D, ROBINSON M B, RATHZ T J, WILLIAMS G. Liquidus temperatures and solidification behavior in the copper–niobium system [J]. Acta Materialia, 1998, 46: 3849−3855.

[50] LI D, ROBINSON M B, RATHZ T J. Measurements of liquidus temperatures in the Cu−Nb and Cu−Cr systems [J]. Journal of Phase Equilibria, 2000, 21: 136−140.

[51] REID J S, KOLAWA E, NICOLET M A. Thermodynamics of (Cr, Mo, Nb, Ta, V, or W)−Si−Cu ternary systems [J]. Journal of Materials Research, 1992, 7(9): 2424−2428.

[52] DINSDALE A T. SGTE data for pure elements [J]. Calphad, 1991, 15: 317−425.

[53] REDLICH O, KISTER A T. Thermodynamics of nonelectrolyte solutions [J]. Industrial and Engineering Chemistry, 1948, 40: 345−348.

[54] MUGGIANU Y M, GAMBINO M, BROSS L P. Comparison between calculated and measured thermodynamic data of liquid (Ag, Au, Cu)−Sn−Zn alloys [J]. The Journal of Chemical Physics, 1975, 72: 85−91.

[55] HILLERT M, STAFFANSSON L I. The regular-solution model for stoichiometric phases and ionic melts [J]. Acta Chemica Scandinavica, 1970, 24: 3618−3626.

[56] SUNDMAN B, ÅGREN J. A regular solution model for phases with several components and sublattices, suitable for computer applications [J]. Journal of Physics and Chemistry

of Solids, 1981, 42: 297−301.
[57] HOHENBERG P, KOHN W. Density functional theory [J]. Physical Review, 1964, 136: B864−B871.
[58] KOHN W, SHAM L J. Self-consistent equations including exchange and correlation effects [J]. Physical Review, 1965, 140: A1133−A1138.
[59] BLÖCHL P E. Projector augmented-wave method [J]. Physical Review B, 1994, 50:17953−17979.
[60] KRESSE G, JOUBERT D. From ultrasoft pseudopotentials to the projector augmented-wave method [J]. Physical Review B, 1999, 59: 1758−1775.
[61] KRESSE G, FURTHMÜLLER J. Efficient iterative schemes for ab initio total-energy calculations using a plane-wave basis set [J]. Physical Review B, 1996, 54: 11169−11186.
[62] KRESSE G, FURTHMÜLLER J. Efficiency of ab-initio total energy calculations for metals and semiconductors using a plane-wave basis set [J]. Computational Materials Science, 1996, 6: 15−50.
[63] HU Biao, YUAN Xiao-ming, DU Yong, WANG Jiong, LIU Zi-kui. Thermodynamic reassessment of the Ni−Si−Ti system using a four-sublattice model for ordered/disordered fcc phases supported by first-principles calculations [J]. Journal of Alloys and Compounds, 2017, 693: 344−356.
[64] SUNDMAN B, JANSSON B, ANDERSSON J O. The thermo-calc databank system [J]. Calphad, 1985, 9: 153−190.

Cu−Nb−Si 体系相平衡的实验研究和热力学模拟

周佳强[1,2]，胡 标[1,3]，李奔富[1,3]，杜 勇[2]，汪 炯[2]

1. 安徽理工大学 材料科学与工程学院，淮南 232001；
2. 中南大学 粉末冶金国家重点实验室，长沙 410083；
3. 安徽省纳米碳基材料与环境健康国际联合研究中心，淮南 232001

摘 要：通过关键实验、热力学建模和第一性原理计算相结合的方法研究 Cu−Nb−Si 体系的相平衡关系。制备 16 种三元合金，采用 X 射线衍射仪(XRD)和扫描电子显微镜结合 X 射线能谱仪(SEM−EDS)，测定三相和两相区范围，证实三元化合物 τ_1($Cu_4Nb_5Si_4$)的存在，同时测定 Cu 在 $NbSi_2$ 和 Nb_5Si_3 相中的溶解度，最终确定 Cu−Nb−Si 体系在 600 和 700 ℃的等温截面。基于文献和本工作的实验数据，结合第一性原理计算和 CALPHAD 方法，利用替代模型和亚点阵模型分别描述溶体相和中间化合物，对 Cu−Nb−Si 体系进行热力学计算，最终得到一套自洽的热力学参数。通过计算与实验结果相比较，所获得的热力学参数能再现可靠的实验数据。

关键词：Cu−Nb−Si 体系；热力学模拟；第一性原理计算；CALPHAD 方法

(Edited by Xiang-qun LI)